Discover Oncology

Research

HOTAIR, a ferroptosis-related gene, promotes malignant behavior of breast cancer via sponging miR-206

Wei Wu[1] · Zhihan Yao[1] · Yongxing Chen[1] · Rongxuan Xu[1] · Chenxin Jin[1] · Xiaofeng Li[1]

Received: 5 January 2025 / Accepted: 22 May 2025
Published online: 29 May 2025

Abstract
Ferroptosis, an iron-dependent regulated cell death modality driven by lipid peroxidation cascades, has emerged as a critical pathogenic mechanism in tumorigenesis and therapeutic resistance. The long non-coding RNA HOTAIR (HOX transcript antisense RNA), previously recognized as a key epigenetic modulator in tumor biology, orchestrates malignant phenotypes through regulation of cell cycle dynamics, proliferative signaling, and metastatic potential. Despite these advances, the mechanistic interface between HOTAIR-mediated ceRNA networks and ferroptosis regulation in breast carcinogenesis remains undefined. Bioinformatic analysis and RT-qPCR validation precisely mapped the subcellular localization and interaction networks of this regulatory axis. Key findings revealed that HOTAIR silencing functionally promotes malignant phenotypes (proliferation, migration and invasion), and mechanistically serves as a molecular sponge for miR-206, thereby de-repressing CERS2 expression to modulate ferroptosis susceptibility. Given the established correlation between HOTAIR silencing and ferroptosis in BRCA, our data suggest that pharmacological induction of ferroptosis represents a promising therapeutic paradigm for this molecular subset. This work not only deciphers a novel HOTAIR/miR-206/CERS2 axis in ferroptosis regulation but also provides translational insights for developing biomarker-driven treatment strategies in refractory breast malignancies.

Keywords Breast cancer · Ferroptosis · CeRNA · HOTAIR · Regulation

Abbreviations

BRCA	Breast cancer
DEGs	Different expressive genes
DEFRLs	Different expressive ferroptosis-related lncRNAs
ceRNA	Competitive endogenous RNA

1 Introduction

Breast cancer (BRCA) remains the predominant malignancy threatening female health globally, characterized by high morbidity and cancer-related mortality [1]. Epidemiological analyses reveal a concerning upward trajectory in both incidence and mortality rates worldwide, with the disease burden increasingly impacting women's physical and psychological

Supplementary Information The online version contains supplementary material available at https://doi.org/10.1007/s12672-025-02791-x.

✉ Xiaofeng Li, lxf_chen@dmu.edu.cn | [1]Department of Epidemiology and Health Statistics, Dalian Medical University, Dalian, China.

Fig. 1 Identification of ferroptosis-related lncRNAs. **A** Flowchart of this research. **B** Volcano maps of the DEGs(1), DEFRLs(2) and DE miRNAs(3) between BRCA tissues and normal tissues in the TCGA database. **C** The results of GO biological process enrichment, GO cellular component enrichment and GO molecular function enrichment of DEGs. **D** The results of KEGG pathways analysis of DEGs

health [2]. Notably, Global Cancer Statistics 2020 documented a paradigm shift where BRCA incidence (2.26 million cases) surpassed lung cancer (2.2 million cases) for the first time, establishing its status as the most prevalent malignancy [1, 3]. Updated Globocan 2022 data (https://gco.iarc.who.int/) further corroborate this trend, reporting 2.30 million new cases representing 23.8% of female cancer diagnoses. While advancements in early detection modalities and therapeutic strategies have significantly improved 5-year survival rates [4, 5], substantial challenges persist in prognosis prediction and treatment optimization. Timely detection and personalized interventions have proven effective in reducing disease mortality [6, 7], underscoring the imperative for novel therapeutic targets and prognostic biomarkers to enhance clinical outcomes.

Emerging as a potential therapeutic target, ferroptosis represents a mechanistically distinct form of regulated cell death, differentiated from classical apoptosis and necrosis [8, 9]by its iron-dependent lipid peroxide accumulation [10, 11]. This oxidative cell death modality demonstrates significant anti-tumor potential through selective induction in malignant cells [12, 13]. The ferroptotic cascade involves coordinated molecular events including intracellular iron overload, glutathione (GSH) depletion, glutathione peroxidase 4 (GPX4) inactivation, and lethal lipid peroxidation [14–16]. Current research focuses on elucidating the complex regulatory networks involving iron metabolism genes, redox-related proteins, and tissue-specific modulators [17, 18]. Particularly promising are therapeutic strategies targeting ferroptosis induction, which have emerged as a frontier in precision oncology [19–21].

Parallel to these developments, dysregulation of competitive endogenous RNA (ceRNA) networks has been implicated in carcinogenesis and disease progression across multiple malignancies [22–24]. The ceRNA hypothesis proposes a dynamic post-transcriptional regulatory mechanism where RNA transcripts sharing microRNAs (miRNAs) response elements- particularly within their 3′-untranslated regions-compete for miRNA binding, thereby modulating target mRNA expression and phenotypic outcomes [25–27]. Despite growing recognition of both ferroptosis and ceRNA networks in oncobiology, their potential interplay in BRCA prognosis remains underexplored.

To address this knowledge gap, we systematically analyzed the tripartite regulatory axis comprising long non-coding RNAs (lncRNAs), miRNAs, and messenger RNAs (mRNAs). Our findings establish HOTAIR as a critical oncogenic lncRNA in BRCA progression through ferroptosis modulation. Mechanistic investigations reveal that HOTAIR functions as a molecular sponge for miR-206, competitively binding this miRNA to relieve its suppressive effect on ceramide synthase 2 (CERS2). This ceRNA-mediated regulation elevates CERS2 expression, subsequently triggering ferroptotic cell death. These results position the HOTAIR-miR-206/CERS2 axis as a promising therapeutic target for BRCA intervention.

2 Materials and methods

2.1 Gene expression profile data collection

We obtained the expression data and clinical data of BRCA from the Cancer Genome Atlas (TCGA) database (https://cancergenome.nih.gov/). The mRNA and lncRNA expression data consisted of 1231 samples, including 1118 BRCA tissues and 113 normal tissues. The miRNA expression data comprised 1207 samples, with 1103 BRCA tissues and 104 normal mammary tissues. Additionally, we acquired clinical data for 1097 BRCA samples, encompassing survival time, survival status, age, gender, T stage, N stage, M stage, clinical stage, and pathological stage. The FerrDb database (http://www.zhounan.org/) was screened to identify a total of 484 Ferroptosis-Related Genes (FRGs). Serving as a pioneering manually curated resource in this field of research study on ferroptosis markers, regulators, and associated diseases.

2.2 Differentially expressed genes analysis

The limma package from R 4.3.1 software was utilized for conducting differential expression analysis on the RNA expression profiles obtained from the TCGA database. We downloaded 484 FRGs from the FerrDb website, which included 369 driver genes, 11 marker genes, and 348 suppressor genes. Subsequently, we employed the cor function to identify

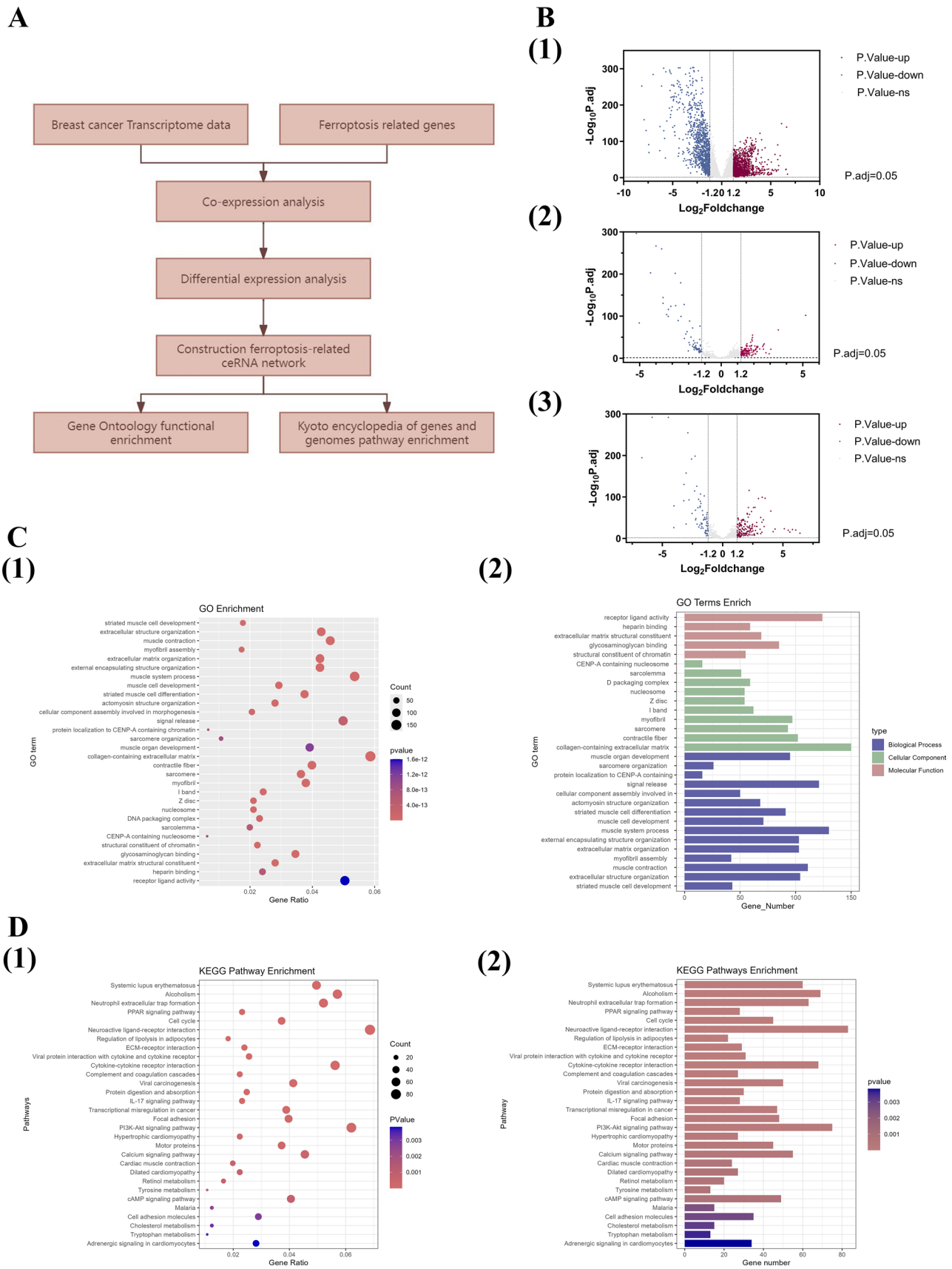
A
Breast cancer Transcriptome data
Ferroptosis related genes
Co-expression analysis
Differential expression analysis
Construction ferroptosis-related ceRNA network
Gene Ontoology functional enrichment
Kyoto encyclopedia of genes and genomes pathway enrichment
B
(1)
(2)
(3)
P.Value-up
P.Value-down
P.Value-ns
P.adj=0.05
-Log10P.adj
Log2Foldchange
C
(1)
GO Enrichment
striated muscle cell development
extracellular structure organization
muscle contraction
myofibril assembly
extracellular matrix organization
external encapsulating structure organization
muscle system process
muscle cell development
striated muscle cell differentiation
actomyosin structure organization
cellular component assembly involved in morphogenesis
signal release
protein localization to CENP-A containing chromatin
sarcomere organization
muscle organ development
collagen-containing extracellular matrix
contractile fiber
sarcomere
myofibril
I band
Z disc
nucleosome
DNA packaging complex
sarcolemma
CENP-A containing nucleosome
structural constituent of chromatin
glycosaminoglycan binding
extracellular matrix structural constituent
heparin binding
receptor ligand activity
GO term
Gene Ratio
Count
pvalue
(2)
GO Terms Enrich
receptor ligand activity
heparin binding
extracellular matrix structural constituent
glycosaminoglycan binding
structural constituent of chromatin
CENP-A containing nucleosome
sarcolemma
D packaging complex
nucleosome
Z disc
I band
myofibril
sarcomere
contractile fiber
collagen-containing extracellular matrix
muscle organ development
sarcomere organization
protein localization to CENP-A containing
signal release
cellular component assembly involved in
actomyosin structure organization
striated muscle cell differentiation
muscle cell development
muscle system process
external encapsulating structure organization
extracellular matrix organization
myofibril assembly
muscle contraction
extracellular structure organization
striated muscle cell development
GO term
Gene_Number
type
Biological Process
Cellular Component
Molecular Function
D
(1)
KEGG Pathway Enrichment
Systemic lupus erythematosus
Alcoholism
Neutrophil extracellular trap formation
PPAR signaling pathway
Cell cycle
Neuroactive ligand-receptor interaction
Regulation of lipolysis in adipocytes
ECM-receptor interaction
Viral protein interaction with cytokine and cytokine receptor
Cytokine-cytokine receptor interaction
Complement and coagulation cascades
Viral carcinogenesis
Protein digestion and absorption
IL-17 signaling pathway
Transcriptional misregulation in cancer
Focal adhesion
PI3K-Akt signaling pathway
Hypertrophic cardiomyopathy
Motor proteins
Calcium signaling pathway
Cardiac muscle contraction
Dilated cardiomyopathy
Retinol metabolism
Tyrosine metabolism
cAMP signaling pathway
Malaria
Cell adhesion molecules
Cholesterol metabolism
Tryptophan metabolism
Adrenergic signaling in cardiomyocytes
Pathways
Gene Ratio
Count
PValue
(2)
KEGG Pathways Enrichment
Pathway
Gene number
pvalue

lncRNAs associated with ferroptosis using a threshold of *P value* < *0.001* and corFilter > 0.4. False discovery rate (FDR) correction was then applied to adjust the P values, and differentially expressed genes (DEGs) were identified based on a criterion of *adj.P value* < *0.05* and | logFC |> 1.2 (fold change difference ratio). Finally, we visualized the DEGs using the "ggplot2" package in R for heatmap, while Graphpad Prism 9 was used for generating the volcano plot.

2.3 Establishment of the ceRNA network

Firstly, miRcode (http://www.mircode.org/) was utilized to predict the targeted miRNAs of differentially expressed lncRNAs, and the outcomes were intersected with DEmiRNA. Subsequently, Targetscan (https://www.targetscan.org/), miRDb (https://mirdb.org/), and miRtarbase (https://mirtarbase.cuhk.edu.cn/) were employed to assess the potential mRNA targets for the identified miRNAs. The results predicted by these databases were considered in conjunction with the intersection set of DEGs. Notably, Targetscan and miRtarbase are renowned databases proficient in predicting mammalian-specific miRNA binding sites. Finally, based on the obtained results, we constructed and visualized the ceRNA network using Cytoscape (version 3.9.0).

2.4 Functional enrichment analysis

Gene Ontology (GO) functional enrichment and Kyoto encyclopedia of genes and genomes (KEGG) pathway enrichment were analyzed by using the 'Cluster Profiler' software package of R software. In GO and KEGG enrichment analysis, P < 0.05 was used as the threshold with statistical significance. The result was visualized by using the "ggplots" package of R software.

2.5 Cell culture and transfection

The MCF-10A, MCF-7, and MDA-MB-231 cell lines were kindly provided by Wuhan Pricella Biotechnology (Wuhan, China). All cell lines were cultured at 37 °C in a 5% CO_2 atmosphere following established protocols. Authentication of all cell lines was conducted through STR profiling and confirmed their absence of mycoplasma contamination.

2.6 RNA extraction and quantitative real-time PCR (qRT-PCR)

RNA was extracted with *AG RNAex Pro* reagent (ACCURATE BIOTECHNOLOGY(HUNAN) CO.,LTD, Changsha, China), and *Evo M-MLV* RT Kit with gDNA Clean for qPCR(ACCURATE BIOTECHNOLOGY(HUNAN) CO.,LTD, Changsha, China) was used for reverse transcription. *2 × SYBR Green Pro Taq HS Premix* (ACCURATE BIOTECHNOLOGY(HUNAN) CO.,LTD, Changsha, China) was used to perform qRT-PCR analysis. Relative RNA expression levels were all measured by the *CFX Connect Real-Time PCR System* (Bio-Rad Laboratories, Singapore).

2.7 Cell transfection

Transfections were performed using Lipofectamine 3000 (Invitrogen) according to the manufacturer's instructions. The plasmids, which contained the siRNAs and the negative control were obtained from Gene Pharma (Shanghai, China). The sequence of si-HOTAIR#1 is: 5′-CCCAUGGACUCAUAAACAATT-3′, and 5′-UUGUUUAUGAGUCCAUGGGTT-3′; si-HOTAIR#2 is: 5′-CCAUACAUUGGGUAGGUAUTT-3′ and 5′-AUACCUACCCAAUGUAUGGTT-3′; the negative control is: 5′-UUCUCCGAA CGUGUCACGUTT-3′ and 5′-ACGUGACACGUUCGGAGAATT-3′. All constructs were confirmed by sequencing.

2.8 Cell proliferation assay

The cell proliferation assay was conducted using a *CCK-8 assay kit* (Seven, Beijing, China). The required cells were seeded in a 96-well plate at a density of 2000 cells per well, one day prior to the experiment. Following cell adhesion, each well was supplemented with 100 µl fresh culture medium and 10 µl of CCK-8 solution and incubated for 2 h at 37 °C. Subsequently, the absorbance was measured spectrophotometrically at 450 nm after incubation for specified time intervals of 24, 48, and 72 h. All experiments were performed in quintuplicate and repeated in triplicate.

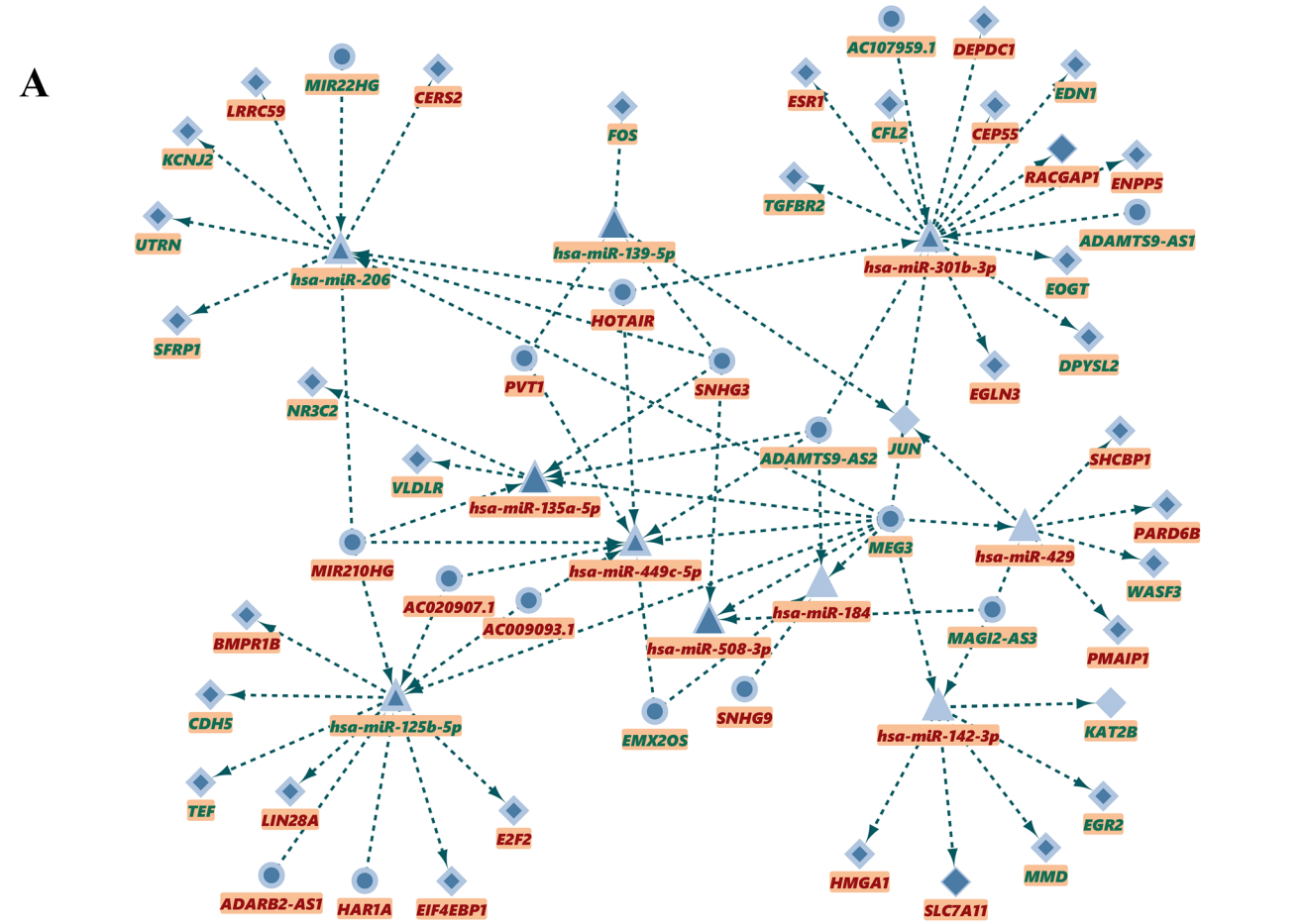

Fig. 2 Construction of ferroptosis-related ceRNA network. **A** The ceRNA networks show the association among DEGs, DEFRLs and DE miRNAs. Red represents upregulated genes and green represents downregulated genes. And rhombus represents DEGs, round shape represents DEFRLs and triangle represents DE miRNAs. **B** The box plots represent the relative expression of genes (HOTAIR (1), has-miR-206(2) and CERS2(3)) in the BRCA tissues and the normal tissues

2.9 Colony formation assay

The colony formation assay was performed by seeding 2000 cells per well into 6-well plates and culturing them in DMEM medium supplemented with 10% FBS for a duration of 2 weeks, with regular replacement of the medium every 4 days. Following fixation in 4% paraformaldehyde for a period of 10 min, the cells were stained using a solution of 1% crystal violet. Colonies exceeding a diameter of 50 μm were enumerated. Each sample was evaluated in triplicate.

Fig. 3 Knockdown of HOTAIR inhibits the proliferation of BRCA cells. **A** HOTAIR expression in BRCA cell lines and the MCF-10A cell line (a normal breast cell line). Cell proliferation of MDA-MB-231 (**B**) and MCF-7 (**C**) with HOTAIR knockdown was assessed by CCK-8 assay. **D**, **E**, **F** Colony formation assays detected the effect of HOTAIR knockdown on cell proliferation ability. The experimental data were expressed as mean ± SEM, *$P < 0.05$, **$P < 0.01$, ***$P < 0.001$

2.10 Cell invasion and migration assays

A transwell system (8.0 μm) was employed for the cell invasion assay. The upper chamber was seeded with cells and cultured in a serum-free medium, while the lower chamber was supplemented with serum medium. To assess cell invasion, the bottom of the upper chamber was coated with Matrigel. After 48 h of cell seeding, cells on the upper surface were gently removed by swabbing, followed by fixation, staining, washing of the cells on the lower surface, and subsequent photography for quantification purposes.

Additionally, a wound-healing scratch assay was conducted to evaluate cellular migration ability. Cells were pre-seeded in a six-well plate one day prior to experimentation. Scratch wounds were created using a 20 μl pipette tip and incubated in a serum-free medium for 24 h. The progress of scratch closure was monitored and photographed at both 0 and 24 h time points using Image J software to measure the distance between two edges of each scratch wound.

2.11 RNA immunoprecipitation (RIP)

The RIP assay was conducted using the RNA Immunoprecipitation (RIP) Kit (Bersin Bio, Guangzhou, China), following the manufacturer's instructions. Briefly, transfected cells were washed twice with ice-cold PBS and lysed in an equal volume of RIP lysis buffer supplemented with a protease inhibitor cocktail and RNase inhibitors. Subsequently, the cell lysates were incubated with immunoprecipitation buffer containing magnetic beads conjugated to anti-Ago2 antibody (Proteintech, China) or negative control anti-IgG antibody (Bersin Bio, Guangzhou, China) at 4 °C overnight. After washing the beads with proteinase K buffer, immunoprecipitated RNAs were extracted and purified for further quantification of target RNAs by RT-qPCR.

2.12 Measurement of cellular ferroptosis levels

The MDA concentrations were measured using a lipid peroxidation assay kit (Nanjing Jiancheng Bioengineering Institute, China) following the manufacturer's protocol. Iron concentrations were quantified using an Iron Colorimetric Assay kit (Applygen, Beijing, China) as per the manufacturer's guidelines.

2.13 Statistical analysis

All statistical analyses were performed using the Graphpad Prism 10. Two-sided P values were calculated, and a threshold of $P < 0.05$ was considered statistically significant. The results are expressed as the mean ± SEM. Statistical significance was assigned at *$P < 0.05$ or **$P < 0.01$.

3 Results

3.1 Construction and analysis of the ferroptosis-related ceRNA network

The overall study design is illustrated in Fig. 1A. Transcriptomic and clinical data for BRCA were retrieved from the TCGA database, with RNA sequences categorized into mRNA and lncRNA subsets based on ensembled identifiers. Through co- expression analysis between FRGs and lncRNAs, we identified 428 ferroptosis-related lncRNAs. Differential expression analysis further revealed 2690 DEGs (1191 downregulated and 1499 upregulated mRNA), 197 differentially expressed ferroptosis-related lncRNAs (DEFRGLs; 66 downregulated and 131 upregulated lncRNAs), as well as 243 differentially expressed miRNAs (DE miRNAs; 73 downregulated and 170 upregulated miRNAs). The distribution of these differentially expressed RNAs was visualized through volcano plots (Fig. 1B) and expression heatmaps (Figure S1A-C).

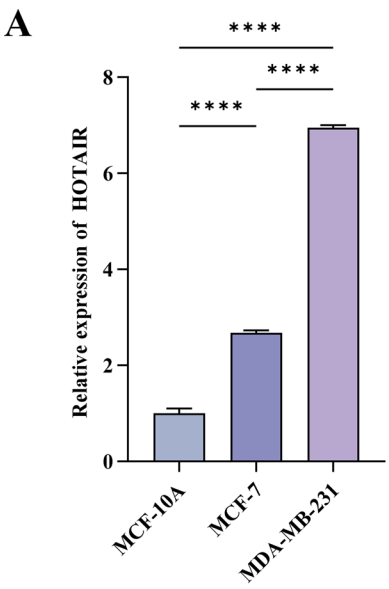
A
****
****
****
Relative expression of HOTAIR
0
2
4
6
8
MCF-10A
MCF-7
MDA-MB-231

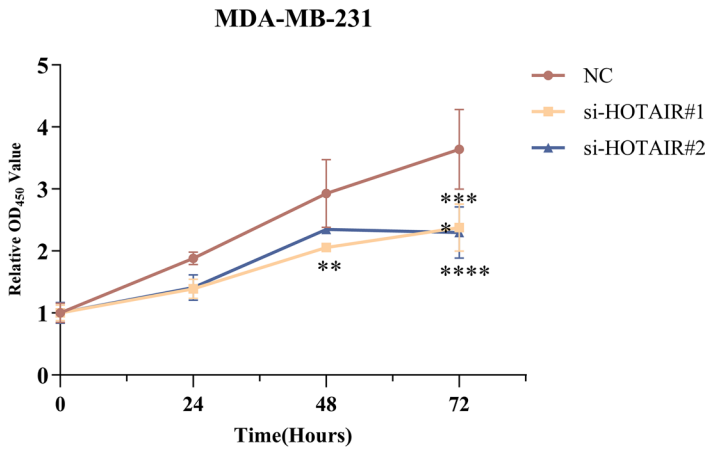
B
MDA-MB-231
NC
si-HOTAIR#1
si-HOTAIR#2
Relative OD450 Value
0
1
2
3
4
5
0
24
48
72
Time(Hours)
**
***
*
****

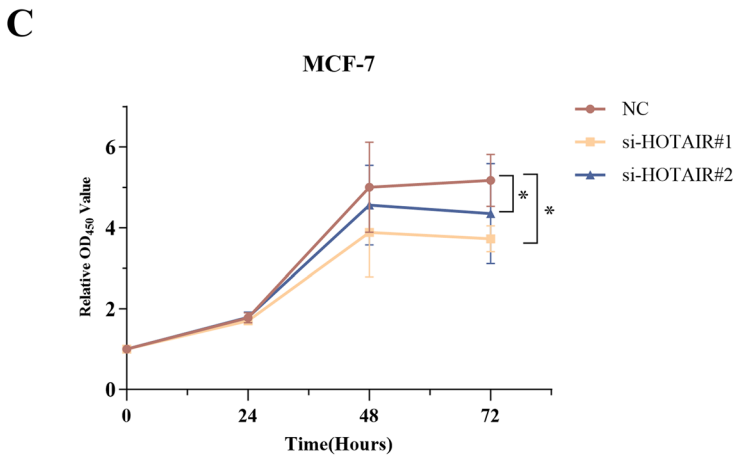
C
MCF-7
NC
si-HOTAIR#1
si-HOTAIR#2
Relative OD450 Value
0
2
4
6
0
24
48
72
Time(Hours)
*
*

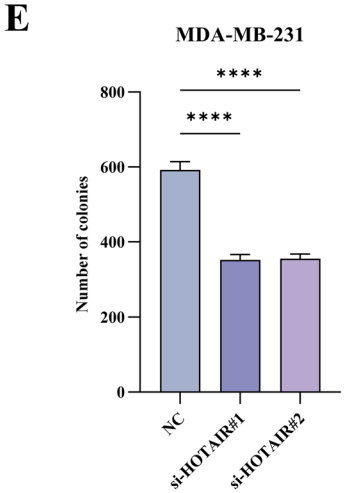
E
MDA-MB-231
****
****
Number of colonies
0
200
400
600
800
NC
si-HOTAIR#1
si-HOTAIR#2

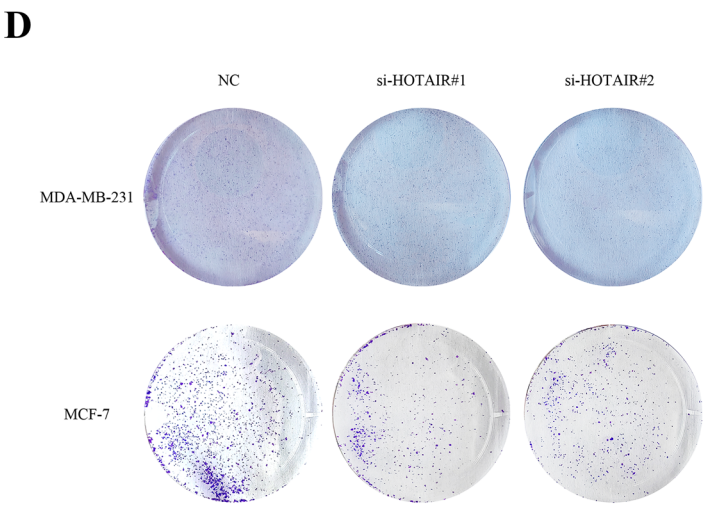
D
NC
si-HOTAIR#1
si-HOTAIR#2
MDA-MB-231
MCF-7

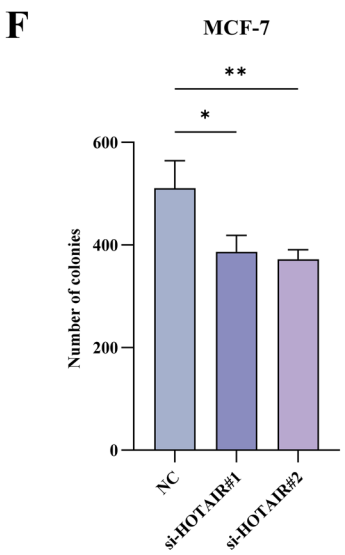
F
MCF-7
**
*
Number of colonies
0
200
400
600
NC
si-HOTAIR#1
si-HOTAIR#2

Fig. 4 Knockdown of HOTAIR inhibits the migration and invasion of BRCA cells. Scratch assays evaluated the migration ability of MDA-MB-231 (**A**, **B**) and MCF-7 (**C**, **D**) cell lines with HOTAIR knockdown. Transwell assay (**E**, **F**) confirmed that invasion ability of MDA-MB-231 cell line was suppressed with HOTAIR knockdown. The experimental data were expressed as mean ± SEM, *$P < 0.05$, **$P < 0.01$, ***$P < 0.001$

Functional enrichment analysis of DEGs yielded 1,400 GO terms (1,204 biological processes [BPs], 107 cellular components [CCs], and 89 molecular functions [MFs]) and 32 KEGG pathways (Fig. 1C, D). BPs predominantly involved extracellular matrix organization, muscle organ development, and processes such as "muscle system process," "signal release," and "muscle contraction." CCs were enriched in structural components including "collagen-containing extracellular matrix," "contractile fiber," and "myofibril," while MFs encompassed "receptor ligand activity," "glycosaminoglycan binding," and transmembrane transporter activities for various amino acids and proteins. KEGG pathway analysis highlighted metabolic pathways and apoptosis-related signaling cascades, notably the "IL-17 signaling pathway," "PI3K-Akt signaling pathway," and "neuroactive ligand-receptor interaction."

To elucidated ferroptosis-associated ceRNA regulatory mechanisms, we first predicted miRNA-lncRNA interactions using the miRcode database, identifying 41 candidate pairs (Table S1). Subsequent miRNA-mRNA targeting via miRDb, miRTarbase, and TargetScan database yielded 36 miRNA-mRNA regulatory pairs. Integration of these interactions enabled the construction of a ceRNA network (Fig. 2A), with the HOTAIR-miR-206-CERS2 axis emerging as a focal regulatory triad for further investigation. Differential expression patterns of these molecules between tumor and normal tissues were validated through box plots (Fig. 2B), while survival analysis demonstrated their prognostic relevance in BRCA (Figure S1D-F).

3.2 HOTAIR promotes BRCA cells proliferation, migration and invasion

Differential expression analysis revealed pronounced upregulation of HOTAIR in breast tumor tissues compares to normal controls. This finding was independently validated by RT-qPCR (Fig. 3A), demonstrating significantly elevated HOTAIR levels in BRCA cell lines (MCF-7: $p < 0.01$; MDA-MB-231: $p < 0.01$) relative to the non-tumorigenic MCF-10A cells. To interrogate HOTAIR's functional role in BRCA progression, we designed two HOTAIR-specific siRNAs (si-HOTAIR#1 and si-HOTAIR#2) alongside a non-targeting control siRNA (si-NC). Transfection efficiency was confirmed by RT-qPCR, with both si-HOTAIR constructs achieving robust knockdown (Figure S2A-B).

Functional characterization through CCK-8 and colony formation assays revealed that HOTAIR silencing significantly attenuated proliferative capacity in MCF-7 and MDA-MB-231 cells. CCK-8 analysis showed progressive suppression of cell viability from 48 to 72 h post-transfection (Fig. 3B, C). Consistently, colony formation assays demonstrated a reduction in clonogenic potential in both cell lines (Fig. 3D–F).

Migration and invasion capacities were systematically evaluated using scratch wound healing and Transwell assays. HOTAIR knockdown reduced wound closure rates compared to si-NC controls at 24 h (Fig. 4A–D). Similarly, Transwell invasion assays revealed a decrease in invasive cell numbers following HOTAIR suppression (Fig. 4E, F). Collectively, these data establish HOTAIR as a potent oncogenic lncRNA driving BRCA progression through coordinated regulation of proliferation, migration, and invasion.

3.3 HOTAIR modulated ferroptosis in BRCA

To delineate HOTAIR's role in ferroptosis regulation, we treated MDA-MB-231 and MCF-7 cells with the ferroptosis inducer Erastin (5 μM, 24 h). RT-qPCR revealed pronouncecd HOTAIR upregulation in Erastin-treated cells compared to untreated controls (Fig. 5A). Functional validation via CCK-8 assays demonstrated that HOTAIR knockdown significantly attenuated Erastin-induced cytotoxicity, with cell viability increasing relative to si-NC-treated cells (Fig. 5B, C).

Considering that Fe^{2+} is crucial for the process of ferroptosis, MDA serves as an important product of lipid ROS, and GSH acts as the primary intracellular antioxidant by scavenging intracellular lipid hydrogen peroxide to prevent ferroptosis; we further quantified their concentrations in erastin-treated BRCA cells. Interestingly, knockdown of HOTAIR significantly inhibited the consumption of GSH (Fig. 5D, E) and accumulation of MDA (Fig. 5F, G) and Fe^{2+} (Fig. 5H, I).

Collectively, these data collectively demonstrate that HOTAIR potentiates Erastin-induced ferroptosis in BRCA by coordinating iron accumulation, GSH exhaustion, and lipid peroxidation, positioning it as a critical regulatory node in ferroptosis execution.

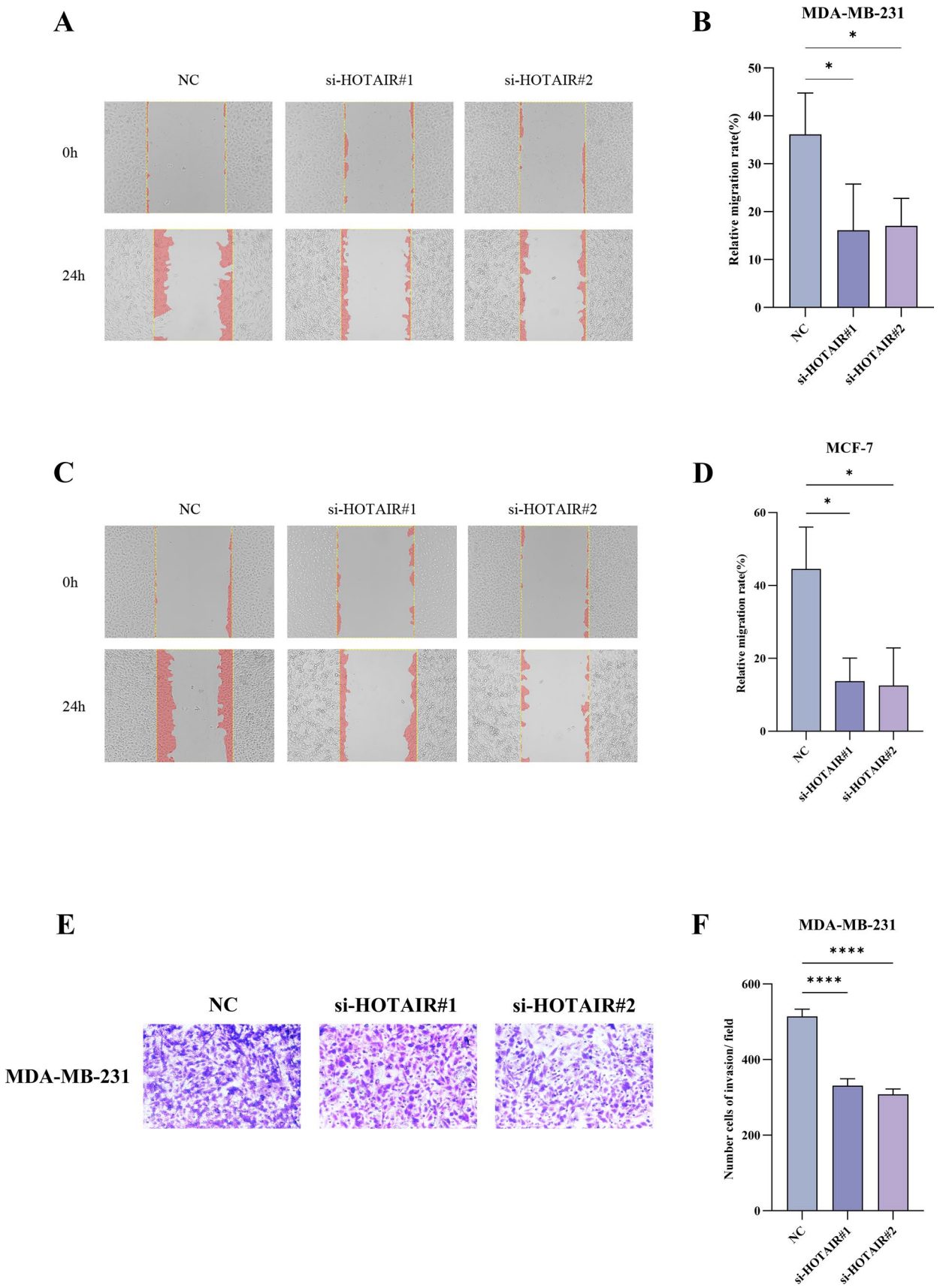
A
NC
si-HOTAIR#1
si-HOTAIR#2
0h
24h
B
MDA-MB-231
*
*
Relative migration rate(%)
50
40
30
20
10
0
NC
si-HOTAIR#1
si-HOTAIR#2
C
NC
si-HOTAIR#1
si-HOTAIR#2
0h
24h
D
MCF-7
*
*
Relative migration rate(%)
60
40
20
0
NC
si-HOTAIR#1
si-HOTAIR#2
E
NC
si-HOTAIR#1
si-HOTAIR#2
MDA-MB-231
F
MDA-MB-231
****
****
Number cells of invasion/ field
600
400
200
0
NC
si-HOTAIR#1
si-HOTAIR#2

Fig. 5 HOTAIR contributed to the ferroptosis in BRCA. MDA-MB-231(1) and MCF-7(2) cell lines transfected with indicated constructs were ▶ treated with erastin (5 μM) for 24 h, and the expression level of HOTAIR was measured by RT-qPCR (**A**). The cell viability was determined with a CCK-8 kit (**B**, **C**), GSH concentration was analyzed using a glutathione assay kit (**D**, **E**), lipid formation was measured by MDA assay (**F**, **G**), and the intracellular Fe2 + was measured by iron detection assay (**H**, **I**). The experimental data were expressed as mean ± SEM, *$P < 0.05$, **$P < 0.01$, ***$P < 0.001$

3.4 HOTAIR drives CERS2 expression through miR-206 sequestration in BRCA

To elucidate the ceRNA mechanism of HOTAIR, we first performed subcellular localization analysis using the lncLocator platform, revealing predominant cytoplasmic enrichment of HOTAIR (Fig. 6A), a prerequisite for miRNA sponging activity. Transcriptomic profiling and RT-qPCR validation identified miR-206 as a candidate interactor, showing significant downregulation in BRCA cell lines compared to normal MCF-10A cells (Fig. 6B). Additionally, as Ago2 is an essential component of the RNA-induced silencing complex (RISC), we performed in MDA-MB-231 and MCF-7 cells to determine whether HOTAIR binds to miR-206 in an Ago2-dependent manner (Fig. 6C, D). Collectively, these results mechanistically establish HOTAIR as a functional miR-206 sponge in BRCA.

We next interrogated the downstream effector of this regulatory axis. RT-qPCR analysis revealed marked CERS2 upregulation in BRCA cells (Fig. 7A). HOTAIR knockdown via si-HOTAIR reduced CERS2 expressive levels, demonstrating transcriptional regulation (Fig. 7B, C). Starbase prediction identified two conserved miR-206 binding sites within the CERS2 3'UTR (Fig. 7D). Furthermore, we performed anti-Ago2 RIP assays in MDA-MB-231 and MCF-7 cells to determine whether miR-206 targets to CERS2 in an Ago2-dependent manner (Fig. 7E, F). This integrated evidence delineates a coherent HOTAIR/miR-206/CERS2 axis, where cytoplasmic HOTAIR competitively binds miR-206 to alleviate its repressive effects on CERS2 translation, thereby driving oncogenic signaling in BRCA.

4 Conclusions

In conclusion, by means of integrated bioinformatics analysis, we have successfully constructed a novel ceRNA network involving HOTAIR/has-miR-206/CERS2 that is closely associated with ferroptosis in BRCA. Notably, all the identified RNAs within this network exhibit significant predictive values for BRCA prognosis. Additionally, our findings suggest a crucial role for HOTAIR in regulating ferroptosis through competitive binding with miR-206 to specifically enhance CERS2 expression in BRCA. The results obtained from this study may contribute to a better understanding of the underlying mechanisms driving BRCA progression and offer potential targets for therapeutic intervention.

5 Discussion

LncRNAs have emerged as master regulators of oncogenesis and therapeutic resistance, primarily through their capacity to orchestrate gene regulatory networks and modulate critical cancer hallmarks [28–30]. Our investigation identifies HOTAIR as a ferroptosis-modulating lncRNA in BRCA, demonstrating its marked upregulation under erastin-induced ferroptotic stress. Mechanistically, HOTAIR functions as a molecular sponge to sequester miR-206, thereby attenuating miR-206-mediated repression of CERS2 and consequently enhancing ferroptosis susceptibility in BRCA cells. This study makes three key conceptual advances: First, we establish the first ceRNA network (HOTAIR/miR-206/CERS2) directly linking lncRNA regulation to ferroptosis in BRCA, addressing a critical knowledge gap in non-apoptotic cell death mechanisms. Second, our multi-omics approach reveals the prognostic stratification power of this tripartite axis, providing a novel biomarker panel beyond single-molecule predictors. Third, we demonstrate that HOTAIR-mediated ferroptosis resistance is reversible through miRNA competition, suggesting druggable targets for therapeutic intervention.

The intersection between lncRNA biology and ferroptosis regulation represents an emerging frontier in cancer therapeutics. Accumulating evidence positions ferroptosis induction as a viable strategy for eliminating therapy-resistant and mesenchymal-transitioned tumor cells [31–35]. Our work extends this paradigm by elucidating HOTAIR's role in ferroptosis modulation, complementing recent discoveries of lncRNA-mediated ferroptosis regulation in hepatic malignancies [30, 36]. Notably, the HOTAIR/miR-206/CERS2 axis identified herein provides mechanistic

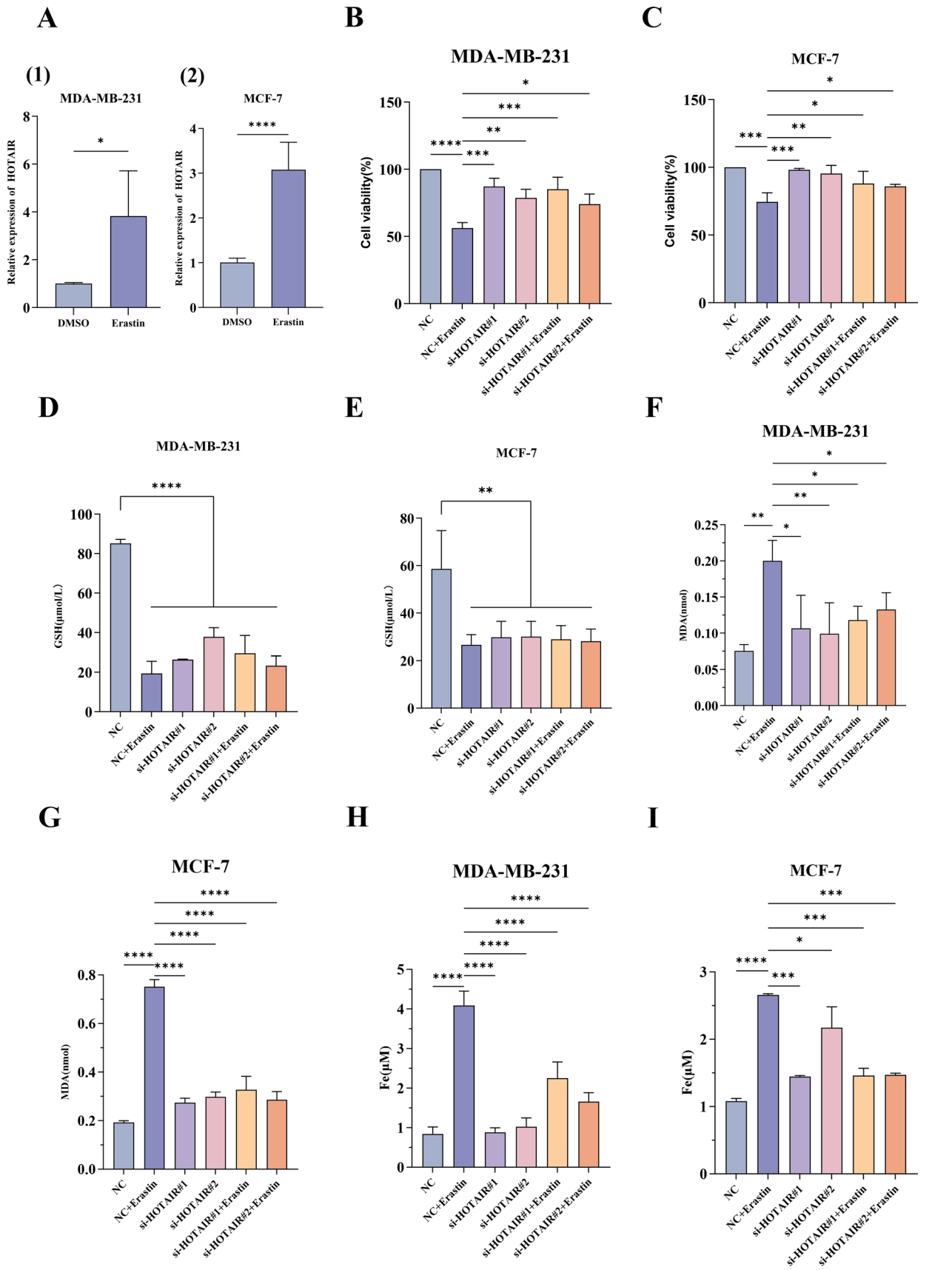
A
(1)
MDA-MB-231
Relative expression of HOTAIR
DMSO
Erastin
(2)
MCF-7
Relative expression of HOTAIR
DMSO
Erastin
B
MDA-MB-231
Cell viability(%)
C
MCF-7
Cell viability(%)
NC
NC+Erastin
si-HOTAIR#1
si-HOTAIR#2
si-HOTAIR#1+Erastin
si-HOTAIR#2+Erastin
D
MDA-MB-231
GSH(μmol/L)
E
MCF-7
GSH(μmol/L)
F
MDA-MB-231
MDA(nmol)
G
MCF-7
MDA(nmol)
H
MDA-MB-231
Fe(μM)
I
MCF-7
Fe(μM)

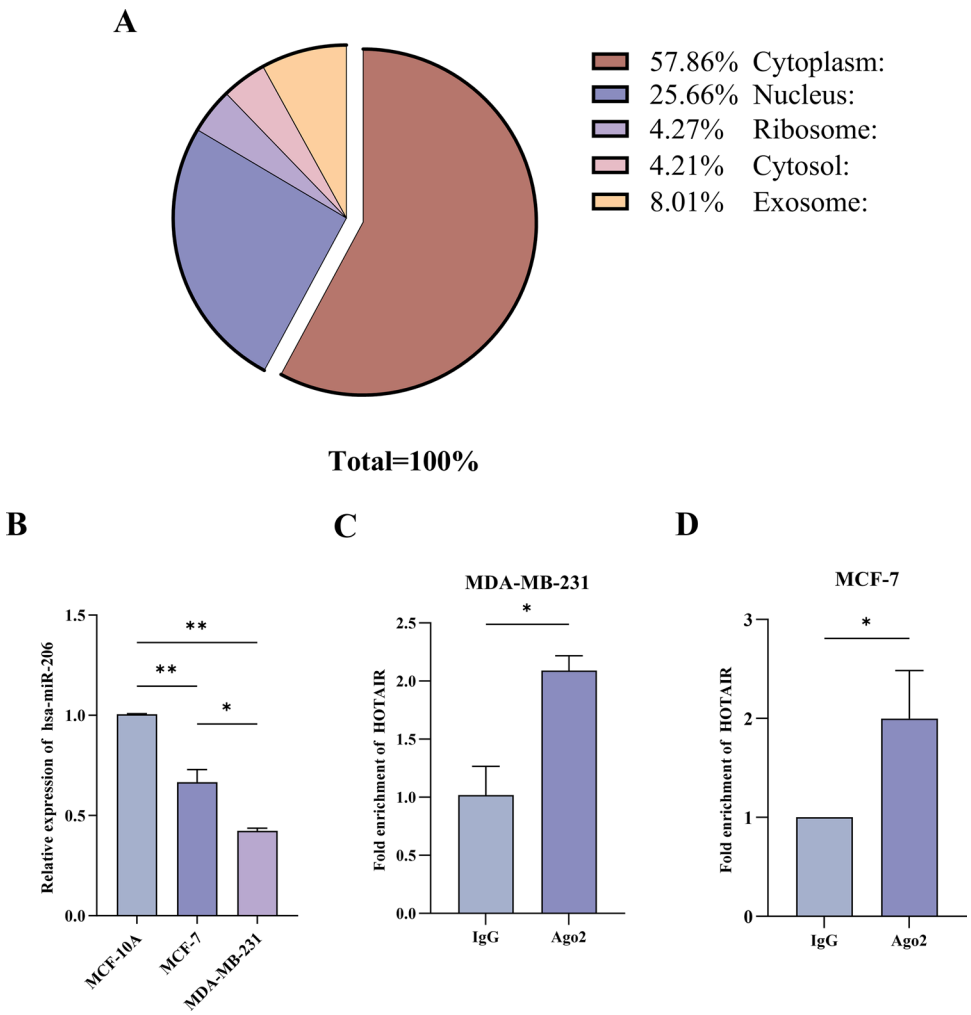

Fig. 6 HOTAIR positively regulates CERS2 expression via sponging miR-206 in BRCA cells. **A** The pie chart shows the subcellular localization of HOTAIR. Has-miR-206 (**B**) expression levels in BRCA cell lines and the MCF-10A cell line (a normal breast cell line). RIP assays (**C**, **D**) confirmed the interaction of HOTAIR-has-miR-206 in BRCA cells. *The experimental data were expressed as mean ± SEM, *P < 0.05, **P < 0.01, ***P < 0.001*

insights distinct from established pathways involving SLC7A11 ubiquitination or palmitoylation [30, 36], suggesting tissue-specific regulatory networks in ferroptosis execution.

Several limitations warrant consideration in interpreting these findings. First, while our bioinformatics analyses incorporated multiple BRCA cohorts, experimental validation was limited to in vitro models, necessitating future investigations using patient-derived xenografts or transgenic mouse models. Second, while we identified HOTAIR as a regulator of CERS2, the correlation between their expression levels (Fig. 7) suggests potential involvement of additional regulatory mechanisms. These may include post-transcriptional modifications, epigenetic modifiers, or compensatory interactions with other RNA-binding proteins that could modulate CERS2 stability or translation efficiency. Third, the study focused on miR-206/CERS2 as downstream effectors, though other miRNAs (e.g., miR-34a, miR-21) known to interact with HOTAIR may contribute to ferroptosis regulation. Fourth, the clinical translation potential requires further pharmacokinetic studies to assess HOTAIR-targeting feasibility. Lastly, the p53-HOTAIR crosstalk observed in MCF-7 cells [37] needs validation across BRCA molecular subtypes given p53's context-dependent roles [38].

Central to ferroptosis regulation is the iron-dependent accumulation of lipid peroxides, a process pharmacologically triggered by erastin through system Xc- inhibition and subsequent glutathione depletion [10, 39, 40]. The pleiotropic tumor suppressor p53 emerges as a key contextual modulator of ferroptotic sensitivity, exhibiting dual regulatory roles through cell type-specific mechanisms [38, 41]. Our findings resonate with Xie et al.'s demonstration of p53-mediated ferroptosis resistance in colorectal cancer [42], particularly when considered alongside Yu et al.'s report of HOTAIR depletion upregulating p53 in MCF-7 cells [37]. This p53-HOTAIR regulatory interplay may partially explain the observed ferroptosis potentiation, though further investigation is warranted to delineate potential crosstalk between ceRNA networks and p53 signaling in BRCA.

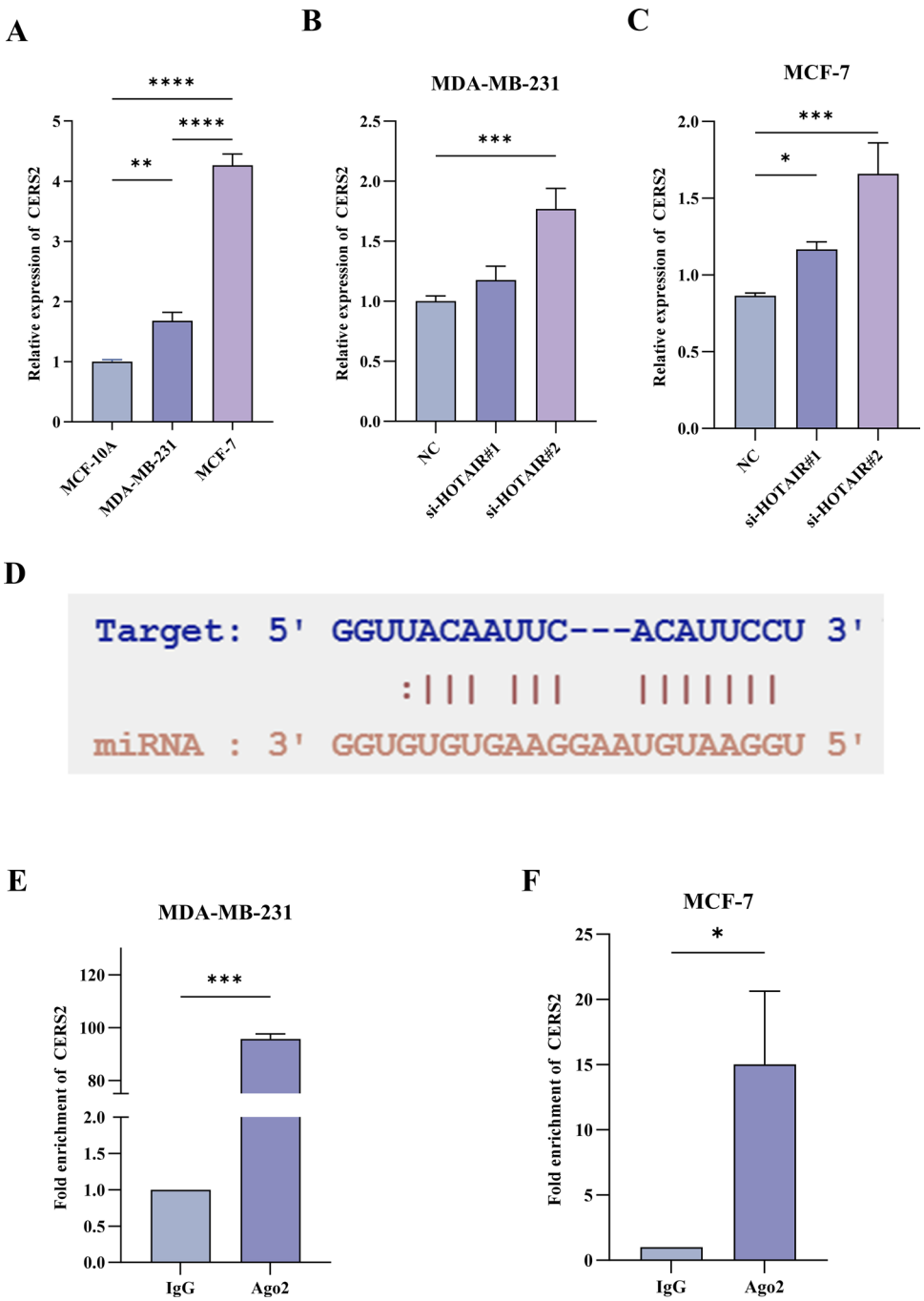

Fig. 7 HOTAIR positively regulates CERS2 expression via sponging miR-206 in BRCA cells. **A** CERS2 expression levels in BRCA cell lines and the MCF-10A cell line (a normal breast cell line). **B**, **C** The expression level of CERS2 in each group transfected as indicated was verified through RT-qPCR. **D** The binding sites between miR-206 and CERS2 were predicted by Starbase database. RIP assays (**E**, **F**) confirmed the interaction of has-miR-206-CERS2 in BRCA cells. *The experimental data were expressed as mean ± SEM, *P < 0.05, **P < 0.01, ***P < 0.001*

Clinically, the HOTAIR-driven ferroptosis resistance mechanism holds dual implications. First, it provides a molecular rationale for the poor prognosis associated with HOTAIR overexpression in chemotherapy-resistant tumors [43]. Second, it suggests therapeutic synergism between ferroptosis inducers and conventional therapies, as evidenced by recent breakthroughs in overcoming drug resistance [40]. The intricate balance between ferroptosis, apoptosis, and autophagy in tumor cell survival underscores the need to elucidate HOTAIR's multimodal regulatory functions—an endeavor critical for developing lncRNA-targeted therapies against cell death-resistant malignancies.

Author contributions W.W. and X.L designed the manuscript. W.W., Z.Y., Y.C., R.X. and C.J. integrated and analyzed the data. W.W. drafted the manuscript. X.L. revised the manuscript. All authors contributed to the article and reviewed the manuscript.

Funding This study was supported by the Foundation of Liaoning Province Education Administration (No. LJKZ0849).

Data availability Data is provided within the manuscript or supplementary information files.

Declarations

Ethics approval and consent to participate Not applicable.

Competing interests The authors declare no competing interests.

References

1. Sung H, Ferlay J, et al. Global cancer statistics 2020: GLOBOCAN estimates of incidence and mortality worldwide for 36 cancers in 185 countries. CA Cancer J Clin. 2021;71(3):209–49.
2. Trapani D, Ginsburg O, et al. Global challenges and policy solutions in breast cancer control. Cancer Treat Rev. 2022;104:102339.
3. Momenimovahed Z, Salehiniya H. Epidemiological characteristics of and risk factors for breast cancer in the world. Breast Cancer. 2019;11:151–64.
4. Chandrashekar DS, Karthikeyan SK, et al. UALCAN: an update to the integrated cancer data analysis platform. Neoplasia. 2022;25:18–27.
5. Farkas AH, Nattinger AB. Breast cancer screening and prevention. Ann Intern Med. 2023;176(11):itc161–76.
6. Chen W, Hoffmann AD, et al. Organotropism: new insights into molecular mechanisms of breast cancer metastasis. NPJ Precis Oncol. 2018;2(1):4.
7. Rahman WT, Helvie MA. Breast cancer screening in average and high-risk women. Best Pract Res Clin Obstet Gynaecol. 2022;83:3–14.
8. Jiang X, Stockwell BR, Conrad M. Ferroptosis: mechanisms, biology and role in disease. Nat Rev Mol Cell Biol. 2021;22(4):266–82.
9. Mou Y, Wang J, et al. Ferroptosis, a new form of cell death: opportunities and challenges in cancer. J Hematol Oncol. 2019;12(1):34.
10. Djulbegovic MB, Uversky VN. Ferroptosis—an iron- and disorder-dependent programmed cell death. Int J Biol Macromol. 2019;135:1052–69.
11. Zheng D, Liu J, et al. ROS-triggered endothelial cell death mechanisms: focus on pyroptosis, parthanatos, and ferroptosis. Front Immunol. 2022;13:1039241.
12. Hassannia B, Vandenabeele P, Vanden Berghe T. Targeting ferroptosis to iron out cancer. Cancer Cell. 2019;35(6):830–49.
13. Badgley MA, Kremer DM, et al. Cysteine depletion induces pancreatic tumor ferroptosis in mice. Science. 2020;368(6486):85–9.
14. Ursini F, Maiorino M. Lipid peroxidation and ferroptosis: the role of GSH and GPx4. Free Radic Biol Med. 2020;152:175–85.
15. Yang WS, SriRamaratnam R, et al. Regulation of ferroptotic cancer cell death by GPX4. Cell. 2014;156(1–2):317–31.
16. Liang D, Feng Y, et al. Ferroptosis surveillance independent of GPX4 and differentially regulated by sex hormones. Cell. 2023;186(13):2748-2764.e22.
17. Tang D, Chen X, et al. Ferroptosis: molecular mechanisms and health implications. Cell Res. 2021;31(2):107–25.
18. Li D, Wang Y, et al. CST1 inhibits ferroptosis and promotes gastric cancer metastasis by regulating GPX4 protein stability via OTUB1. Oncogene. 2023;42(2):83–98.
19. Zhang C, Liu X, et al. Ferroptosis in cancer therapy: a novel approach to reversing drug resistance. Mol Cancer. 2022;21(1):47.
20. Lei G, Zhuang L, Gan B. Targeting ferroptosis as a vulnerability in cancer. Nat Rev Cancer. 2022;22(7):381–96.
21. Zhao L, Zhou X, et al. Ferroptosis in cancer and cancer immunotherapy. Cancer Commun (Lond). 2022;42(2):88–116.
22. Lin C, Ma M, et al. The N(6)-methyladenosine modification of circALG1 promotes the metastasis of colorectal cancer mediated by the miR-342-5p/PGF signalling pathway. Mol Cancer. 2022;21(1):80.
23. Qi X, Lin Y, et al. Decoding competing endogenous RNA networks for cancer biomarker discovery. Brief Bioinform. 2020;21(2):441–57.
24. Braga EA, Fridman MV, et al. LncRNAs in ovarian cancer progression, metastasis, and main pathways: ceRNA and alternative mechanisms. Int J Mol Sci. 2020;21(22):8855.
25. Tay Y, Rinn J, Pandolfi PP. The multilayered complexity of ceRNA crosstalk and competition. Nature. 2014;505(7483):344–52.
26. Salmena L, Poliseno L, et al. A ceRNA hypothesis: the rosetta stone of a hidden RNA language? Cell. 2011;146(3):353–8.
27. Yang S, Wang X, et al. ncRNA-mediated ceRNA regulatory network: transcriptomic insights into breast cancer progression and treatment strategies. Biomed Pharmacother. 2023;162:114698.
28. Li S, Wang X, et al. Identification of the regulatory role of lncRNA HCG18 in myasthenia gravis by integrated bioinformatics and experimental analyses. J Transl Med. 2021;19(1):468.
29. Herman AB, Tsitsipatis D, Gorospe M. Integrated lncRNA function upon genomic and epigenomic regulation. Mol Cell. 2022;82(12):2252–66.

30. Zhang B, Bao W, et al. LncRNA HEPFAL accelerates ferroptosis in hepatocellular carcinoma by regulating SLC7A11 ubiquitination. Cell Death Dis. 2022;13(8):734.
31. Stockwell BR, Jiang X, Gu W. Emerging mechanisms and disease relevance of ferroptosis. Trends Cell Biol. 2020;30(6):478–90.
32. Chen X, Kang R, et al. Broadening horizons: the role of ferroptosis in cancer. Nat Rev Clin Oncol. 2021;18(5):280–96.
33. Zhang H, Deng T, et al. CAF secreted miR-522 suppresses ferroptosis and promotes acquired chemo-resistance in gastric cancer. Mol Cancer. 2020;19(1):43.
34. Bebber CM, Thomas ES, et al. Ferroptosis response segregates small cell lung cancer (SCLC) neuroendocrine subtypes. Nat Commun. 2021;12(1):2048.
35. Sun X, Niu X, et al. Metallothionein-1G facilitates sorafenib resistance through inhibition of ferroptosis. Hepatology. 2016;64(2):488–500.
36. Shi Z, Li Z, et al. Loss of LncRNA DUXAP8 synergistically enhanced sorafenib induced ferroptosis in hepatocellular carcinoma via SLC7A11 de-palmitoylation. Clin Transl Med. 2023;13(6): e1300.
37. Yu Y, Lv F, et al. HOTAIR may regulate proliferation, apoptosis, migration and invasion of MCF-7 cells through regulating the P53/Akt/JNK signaling pathway. Biomed Pharmacother. 2017;90:555–61.
38. Xu R, Wang W, Zhang W. Ferroptosis and the bidirectional regulatory factor p53. Cell Death Discov. 2023;9(1):197.
39. Dixon SJ, Lemberg KM, et al. Ferroptosis: an iron-dependent form of nonapoptotic cell death. Cell. 2012;149(5):1060–72.
40. Deng SH, Wu DM, et al. miR-324-3p reverses cisplatin resistance by inducing GPX4-mediated ferroptosis in lung adenocarcinoma cell line A549. Biochem Biophys Res Commun. 2021;549:54–60.
41. Jiang L, Kon N, et al. Ferroptosis as a p53-mediated activity during tumour suppression. Nature. 2015;520(7545):57–62.
42. Xie Y, Zhu S, et al. The tumor suppressor p53 limits ferroptosis by blocking DPP4 activity. Cell Rep. 2017;20(7):1692–704.
43. Gupta RA, Shah N, et al. Long non-coding RNA HOTAIR reprograms chromatin state to promote cancer metastasis. Nature. 2010;464(7291):1071–6.